Comparative Analysis of Ground-Based and Satellite-Derived UV Index Levels in Natal, Brazil

Gabriela Cacilda Godinho dos Reis, Hassan Bencherif, Rodrigo Silva, Lucas Vaz Peres, Marco Antonio Godinho dos Reis, Damaris Kirsch Pinheiro, Francisco Raimundo da Silva, Kevin Lamy, Thierry Portafaix

remote sensing

MDPI

Article

Comparative Analysis of Ground-Based and Satellite-Derived UV Index Levels in Natal, Brazil

Gabriela Cacilda Godinho dos Reis [1,2,*], Hassan Bencherif [1], Rodrigo Silva [3], Lucas Vaz Peres [3], Marco Antonio Godinho dos Reis [4], Damaris Kirsch Pinheiro [5], Francisco Raimundo da Silva [6], Kevin Lamy [1] and Thierry Portafaix [1,7]

1 Laboratoire de l'Atmosphère et des Cyclones, LACy, UMR 8105 CNRS, Physics Department, Faculty of Sciences and Technologies, Université de La Réunion, Météo-France, 97400 Saint-Denis de La Réunion, France; hassan.bencherif@univ-reunion.fr (H.B.); kevin.lamy@univ-reunion.fr (K.L.); thierry.portafaix@univ-reunion.fr (T.P.)
2 Programa de Pós-Graduação em Sociedade, Natureza e Desenvolvimento, Universidade Federal do Oeste do Pará, Santarém 68035110, Brazil
3 Instituto de Engenharia e Geociências, Universidade Federal do Oeste do Pará, Santarém 68035110, Brazil; rodrigo.silva@ufopa.edu.br (R.S.); lucas.peres@ufopa.edu.br (L.V.P.)
4 Programa de Pós-Graduação em Meteorologia, Universidade Federal de Santa Maria, Santa Maria 97105900, Brazil; reis.marco@acad.ufsm.edu.br
5 Centro de Tecnologia, Departamento de Engenharia Química, Universidade Federal de Santa Maria, Santa Maria 97105900, Brazil; damaris@ufsm.br
6 Instituto Nacional de Pesquisas Espaciais, Natal 66077830, Brazil; francisco.raimundo@inpe.br
7 Institut de Recherche pour le Développement, IRD, DRIE, Antananarivo 101, Madagascar
* Correspondence: gabriela.godinho-dos-reis@univ-reunion.fr or gabriela.reis@discente.ufopa.edu.br; Tel.: +33-262-693-51-73-18

Abstract: The ultraviolet radiation index (UV index–UVI) is a dimensionless indicator that informs the intensity of ultraviolet radiation on the Earth's surface. It makes it easier for people to assess UV levels and understand how to protect themselves from excessive Sun exposure. In Brazil, however, the information regarding UV is scarce, with low spatial and temporal coverage. Thus, continuous monitoring is conducted through satellites, although ground-based monitoring of UV is more accurate than satellite retrievals, and comparisons are necessary for validation. This paper aims to compare the levels of UV index measured on the ground and by satellite (OMI and GOME-2) over Natal, Brazil (05.78°S; 35.21°W) from 2005 to 2022. The comparison was made under clear-sky conditions using METAR cloud cover and LER data. Characterization of the diurnal and seasonal variability of the ground-based UV index levels under all and clear-sky conditions is also reported. The analysis indicates that in Natal, noontime all-sky UV index were 6.8% higher during periods of prevalent broken clouds. The two satellite sources (OMI noontime and overpass) and GOME-2 noontime are reliable sources for UV index, which show good agreement with ground-based measurements, with UVI estimated from OMI both at the overpass and noontime being less biased than GOME-2-estimated UVI. Such a process of data verification is important should these data be used for long-term trend analysis or the monitoring of UV exposure risk and possible impacts on human health.

Keywords: solar ultraviolet radiation; UV index; ground-based measurements; satellite-derived data; OMI; GOME-2; cloud cover; Brazil

Citation: dos Reis, G.C.G.; Bencherif, H.; Silva, R.; Vaz Peres, L.; dos Reis, M.A.G.; Pinheiro, D.K.; da Silva, F.R.; Lamy, K.; Portafaix, T. Comparative Analysis of Ground-Based and Satellite-Derived UV Index Levels in Natal, Brazil. *Remote Sens.* **2024**, *16*, 4687. https://doi.org/10.3390/rs16244687

Academic Editor: Chang-Keun Song

Received: 4 December 2023
Revised: 2 January 2024
Accepted: 3 January 2024
Published: 16 December 2024

1. Introduction

Solar ultraviolet radiation (UV) corresponds to electromagnetic waves with wavelengths of 100–400 nm, constituting approximately 5% of the energy emitted by the Sun [1]. The risks and benefits of exposure to UV for life on Earth have been known for many years [2–4] and include impacts on human health [5–9], materials [10,11], terrestrial and aquatic ecosystems [12–14], and biogeochemical cycles [15,16]. The benefits and detrimental

effects of UV depend on the time of exposure and several other factors, the relative importance of which depends strongly on the highly spatiotemporal UV variability, which is influenced by Sun elevation, total ozone, cloud cover, aerosols, albedo, and altitude [17–19]. Less important factors controlling UV include the ozone profile, trace gases, seasonal changes in the Earth–Sun distance, changes in solar activity, and volcanic eruptions [4,20].

UV is divided into three regions, closely associated with the biological effect of the different wavelengths: UV–A (315–400 nm), UV–B (280–315 nm), and UV–C (100–280 nm) [21–23]. As sunlight passes through the atmosphere, all UV–C and approximately 90% of UV–B are absorbed by ozone, water vapor, oxygen, and carbon dioxide, while UV–A is less affected by the atmosphere [21–24]. Therefore, the UV radiation reaching the Earth's surface is largely composed of UV–A (94%) with a small UV–B component (6%) [25,26].

Diseases related to the accumulation of exposure to UV, like skin cancer and cataracts, are largely preventable with proper Sun protection [25]. Given the need for this type of information, the World Health Organization (WHO) released the ultraviolet index—UVI (UV index)—a dimensionless indicator that provides the amount of UV that reaches the Earth's surface and has varying values on a scale from 0 to 11 or more [25]. Based on this scale, the WHO defines five exposure categories, ranging from low to extreme, with recommended protections at each level. The UV index is an important resource that increases public awareness of the risks of overexposure to the Sun [27].

Brazil is a country of continental dimensions with a large heterogeneity of climates and massive mixing of the population with almost the entire national territory located between the equator and the Tropic of Capricorn, where the Earth's axial tilt to the south makes it one of the countries of the world with the greatest extent of land in proximity to the Sun [28]. Due to geographic characteristics and cultural trends, Brazilians are among the people with the highest annual exposure to the Sun [28]. For the 2020–2022 triennium, in Brazil, about 177,000 new cases of non-melanoma skin cancer were estimated by the Brazilian National Cancer Institute [29]. Non-melanoma skin cancer is the most common type of cancer in men in the south, central west, and southeast regions [29]. In the northeast and north, it ranks second [29]. For women, non-melanoma skin cancer is the most common in all Brazilian regions [29]. Cataracts are the leading cause of blindness and low vision in Brazil [30]. An annual GDP (Gross Domestic Product) loss of more than USD 9 million has been estimated for Latin America and the Caribbean due to blindness and vision impairment, in contrast to just over USD 3 million if education and prevention programs to address risk factors (such as about prolonged and unprotected exposure to UV) were put into practice [30].

In middle-income countries like Brazil, networks and instruments for monitoring UV are often sparse and poorly supported in terms of capacity and funding, and thus, obtaining reliable UV data is difficult. The northern and central–western regions of Brazil have no stations reporting long-term UV series. Of the few studies published on UV variability in Brazilian cities, most were conducted in the southeast and, second, the northeast. An important UV monitoring site in northeastern Brazil is Natal, which is along the Brazilian coastline. Measurements of the UV index in Natal from 2001 to 2007 made using a GUV-511 C surface radiometer were used to produce the curves of hourly mean values for all days between 2001 and 2007 and monthly mean values for the same period by [31]. Their results showed that in Natal, high UV index levels happened before 9:30 a.m. (local time) during all the studied years [31]. Other studies on UV in Natal are available [27,32,33].

Even though Natal is one of the only cities in Brazil where UV has been monitored for more than 10 years, they still do not report data on cloud cover from ground-based imagers. Clouds are important regulators of the radiance balance of the Earth's atmosphere system [34]. The influence of clouds is difficult to accurately account for because they attenuate and enhance UV [35,36]. During cloudy days, they can notably reduce UV at the surface [37]. On days with the partial presence of clouds, UV can be greater than in clear-sky conditions (e.g., UV enhancement under broken clouds) [35–37]. Traditionally, cloud cover is observed from the ground by human observers [38,39] (e.g., METAR, the regular aerodrome weather report). With the advent of new technologies, cloud observations

have been improved using automatic ground-based and orbital imagers [39]. Satellites provide the opportunity for systematic and continuous observation of cloud cover over large spatial scales [40] and provide other ways for cloud characterization, such as using LER (Lambertian equivalent reflectivity). LER can be used for cloud characterization to select clear-sky days for the comparison of ground-based and satellite-derived UV index levels at South African sites [41].

With only a few stations reporting long-term UV measurements in several countries, which significantly restricts its extrapolations to all populated areas [42], a way for continuous UV monitoring on a global scale is through satellites, although ground-based monitoring of UV is more accurate than satellite retrievals [32,43]. Satellite measurements, similar to ground-based observations, are not only affected by instrument errors but are also subject to uncertainties in the algorithms used to derive surface UV radiation [44,45]. Therefore, evaluation of satellite-based estimates of surface UV against available ground measurements at many locations around the world is needed to characterize the errors and further refine the surface UV estimates [45], especially in the southern hemisphere, where there has been relatively limited work to compare ground-based and satellite-derived UV [46].

Given these complexities, the main objective of this study is to conduct a comparative analysis of the ground-based and satellite-derived solar UV indices for Natal, Brazil. Two objectives were identified: (1) to characterize the time variability of the ground-based derived UV index levels in Natal from 2006 to 2022 under all and clear-sky conditions; (2) to compare ground-based and satellite-derived UV index levels in Natal using 2 different techniques to select clear-sky conditions.

Until now, the entire dataset measured by the ground-based Davis 6490 UV sensor used in this research has not been analyzed or compared to satellite-estimated UV index data for the same site. A process of data verification is important to ensure that these data can be used for long-term trend analysis or for monitoring UV exposure risks and potential impacts on human health. In addition, since cloudy conditions pose difficulties with comparisons between ground-based and satellite-derived UV [47], clear-sky conditions offer a more consistent and controlled scenario, eliminating the variable attenuation effects of clouds on UV, which ensures that any differences observed between the two sets of measurements can be attributed more directly to the sensors themselves rather than to other atmospheric conditions. Even more, comparing satellite-derived data with ground-based measurements helps in validating the accuracy of satellite data, which can help identify any discrepancies and improve the satellite data retrieval algorithms, leading to more accurate satellite-derived UV products.

Using these different instruments and techniques, this research promotes a greater understanding of both the variability of UV in Natal, based on different data sources, and the limitations of the instruments and techniques themselves. Also, it is important to highlight that this study contributes to the scientific understanding of UV radiation levels in South America's tropical region, where until now, there has been relatively limited research focusing on this field of study.

2. Materials and Methods

The main aim of this paper is to conduct a comparative analysis of ground-based and satellite-derived UV index levels from OMI and GOME-2 in Natal, Brazil (05.78°S; 35.20°W, 30 m above sea levels (a.s.l)), under clear-sky conditions. To this end, hourly ground-based UV index and daily time series of UV index at noontime and overpass time obtained from the OMI (Ozone Monitoring Instrument) on board the AURA satellite and UV index at noontime derived from GOME-2 instrument (Global Ozone Monitoring Experiment) on board the Metop-A/B/C satellites were used. All the satellite data are available online and free for download through the websites listed in Table 1.

Table 1. Satellite-derived data sources.

Satellite	Instrument	Type of Data	Period	Website
AURA	OMI	UV index (Noontime) UV index (Overpass time) LER	January 2005–December 2022	https://giovanni.gsfc.nasa.gov/giovanni/ (accessed on 13 July 2022) https://search.earthdata.nasa.gov/search (accessed on 13 July 2022) https://search.earthdata.nasa.gov/search (accessed on 13 July 2022)
Metop-A/B/C	GOME-2	UV index (Noontime)	January 2008–December 2022	https://safserver.fmi.fi/index.html (accessed on 13 July 2022)

2.1. Site Description

Natal is a tourist city with beautiful beaches and approximately 896,708 inhabitants [48,49] located on the east coast of northeast Brazil (Figure 1). Its proximity to the equator determines great luminosity and high levels of solar radiation [27]. The city is called "Sun City" by its inhabitants due to the high intensity of solar radiation throughout the year [27,50]. In this city, the UV index is classified as "extreme" from October to April and "very high" from May to August [33]. The average annual UV index observed for the 2001–2012 period was 11 (±1.0) [27]. In the daily cycle, the maximum UV index occurs around 11:20 a.m. It is classified as "high" from 9:00 a.m. to 10:00 a.m. (UTC-3), after which the intensity is considered "very high" [27,51]. In Natal, the average annual temperature and relative humidity are, respectively, 26 °C and 77.3% [33]. The annual accumulated precipitation is 1465.4 mm [52]. The rainy season occurs between April and July, with predominance in April (265 mm) [52,53]. The dry season occurs between August and November [53]. The strongest winds are observed in September, and the weakest occur in April [33].

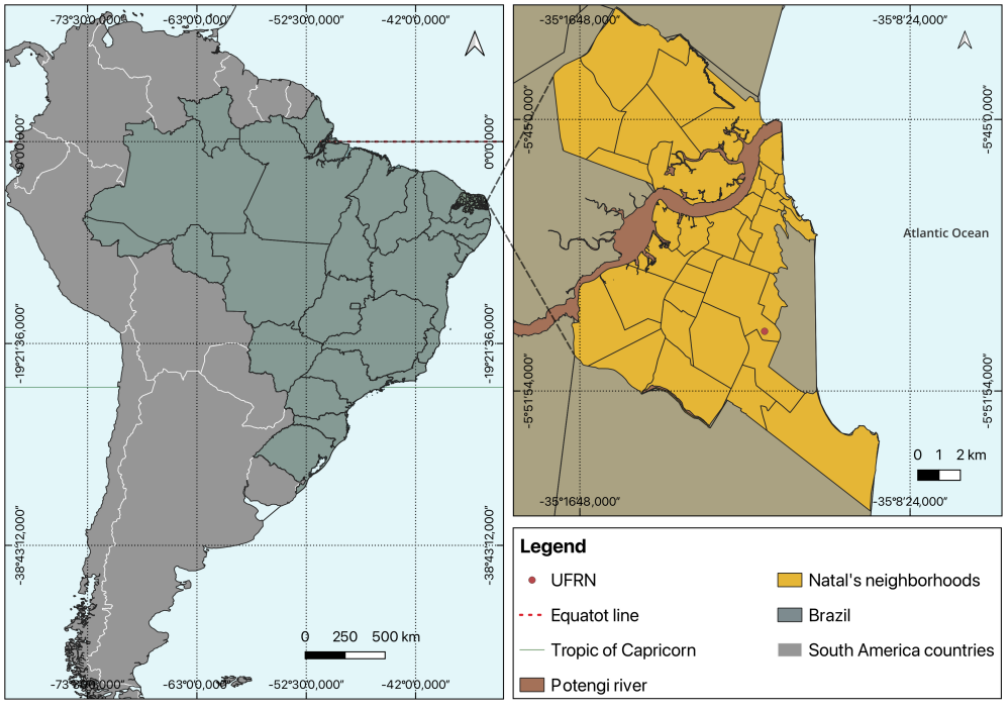

Figure 1. Geographical location of ground−based solar UV sensor in Natal, Rio Grande do Norte, Brazil.

2.2. UV Index

The lower the wavelength in the UV range, the greater the biological response, such that small increases in UV–B irradiance may have substantial biological effects [2,26]. The erythemal action spectrum informs the effectiveness of the wavelengths to produce the

erythema (sunburn) [2]. When UV is weighted by the erythemal action spectrum, it is then named ultraviolet erythemal radiation (UVER) [54,55]. UVER is used to estimate other variables, such as the UV index, standard erythemal doses (SEDs), minimum erythemal doses (MEDs), and Sun exposure time [56]. The UV index (UVI) is a dimensionless indicator, usually divided into five risk categories: UVI $\leq$ 2 (low); 3 $\leq$ UVI $\leq$ 5 (moderate); 6 $\leq$ UVI $\leq$ 7 (high); 8 $\leq$ UVI $\leq$ 10 (very high); and UVI $\geq$ 11 (extreme). This index is defined by Equation (1) [25]:

$$\mathrm{UVI} = K_{er} \int_{250nm}^{400nm} E_{\lambda} S_{er} d\lambda \quad (1)$$

where K_{er} is a scaling factor originally equal to 40 m^2W^{-1}, E_{λ} is the erythemal action spectrum, and S_{er} is the spectral solar irradiance at the surface Wm^2nm^{-1} [25,37].

2.3. Ground-Based Measurements

Monitoring of the UV index in the city of Natal was carried out using the Davis 6490 UV sensor instrument, installed at the Rio Grande do Norte Federal University (UFRN) at an altitude of 30 m a.s.l. This sensor measures the sum of the components of UV transmitted directly and those scattered in the atmosphere [57]. The sensor is a semiconductor photodiode calibrated against a Yankee Environmental Systems' Ultraviolet Pyranometer, model UVB-1, in natural summer daylight [57]. The spectral response is 280 to 360 nm [57], with UV index being one of the sensor outputs with a range from 0 to 16 Index and an accuracy of $\pm$5% [57].

Due to the sensitivity of UV sensors, Davis Instruments recommends recalibration after a period. Since an approximately 2% drift per year on the readings from these sensors is reported [57], the Natal sensor was calibrated every 2 years against a GUV 511 radiometer until 2008. After this period, the GUV 511 used for calibration was sent to another city, and the calibrations in Natal were carried out with a spectrophotometer Brewer 073 until 2017. In 2018, the Davis Sensor was substituted for a brand-new Davis 6490, which is currently in use.

The UV monitored with this sensor covered the years 2006 to 2022, with a sampling frequency of 10 min, which was averaged to the hourly frequency to be used in this study.

2.4. Satellite-Based Instruments

Radiative transfer codes are used for satellites to retrieve UV using ozone, aerosol contents, cloudiness, and surface albedo as input [18]. Some of these inputs, such as ozone and cloudiness, are products of the satellite instrument itself, while aerosol content and albedo come from climatologies [18]. The characteristics of the two satellite instruments that were used in this work (OMI and GOME-2) are detailed below.

2.4.1. Ozone Monitoring Instrument (OMI)

The OMI, onboard NASA's Aura satellite, launched in July 2004 into a Sun-synchronous quasi-polar orbit, is a nadir-viewing UV/visible spectrometer whose mission is the monitoring of atmospheric ozone, trace gases, aerosol, cloudiness, and surface UV [45]. OMI has a spectral resolution of about 0.45 nm in the UV, a wide viewing swath of 2600 km, and a spatial resolution at a nadir of 13 km (along the track) $\times$ 24 km (across-track) [45,58]. The Aura spacecraft circulates in a 98.2° inclination, Sun-synchronous polar orbit at 705 km altitude, with a local afternoon equator crossing time at 13:45 $\pm$ 15 min, providing 14 orbits a day [58,59].

OMI UVI presents a positive bias when compared to ground-based UVI due to, in large part, absorbing aerosols [60–62]. According to [18] and [63], the OMI algorithm version v1.3 applied a correction factor to the algorithm v1.2 that accounts for absorbing aerosols via aerosol climatology, improving the UV estimations. Another uncertainty is added when the satellite overpass happens at a time significantly different from local noon [18] since the OMI UVI given at noontime is estimated using the correction factor estimated at the time

of the overpass [18,61]. The resulting uncertainty of OMI UVI is about 5–10% in clear-sky conditions and about 7–14% in cloudy conditions [18].

2.4.2. Global Ozone Monitoring Experiment (GOME-2)

The GOME-2 is a nadir-viewing scanning UV/VIS spectrometer measuring backscattered and reflected radiation from the Earth's atmosphere in a spectral range between 240 and 790 nm [64,65]. The first GOME-2 was launched in October 2006 onboard the EUMETSAT Metop-A satellite, and a second GOME-2 was launched in September 2012 onboard Metop-B. The long-term dataset was further extended by the third GOME-2 on the Metop-C platform launched in November 2018 [66]. The Metop satellites are flying in Sun-synchronous orbits with equator crossing times of approximately 09:30 LT (local time) and a repeat cycle of 29 days (412 orbits). The summary of the GOME-2 instrument characteristics is in Table 2.

The UV processing algorithm involves the gridding of GOME-2 total ozone data, the inversion of cloud optical depth from reflectance data, and finally, the calculation of surface UV quantities from the radiative transfer model [65]. The GOME-2 UV products include the daily dose and maximum dose rates of integrated UV–B, and UV–A radiation, together with values obtained by different biological weighting functions and solar noon UV index [67].

Table 2. Summary of the GOME-2 instrument characteristics. Retrieved and adapted from [68].

Sensor	GOME-2A	GOME-2B	GOME-2C
Operational Period	January 2007–November 2021	December 2012–Present	January 2019–Present
Spectral Range	240–790 nm	240–790 nm	240–790 nm
Ground Pixel Resolution	80 km × 40 km/40 km × 40 km	80 km × 40 km	80 km × 40 km
Swath Width	1920 km/960 km	1920 km	1920 km
Equator Crossing Time	9:30 (local time)	9:30 (local time)	9:30 (local time)
Global Coverage	1.5 days	1.5 days	1.5 days

The GOME-2 irradiance modeling depends on ozone, surface albedo, cloud, and aerosols; therefore, the uncertainty of GOME-2-derived UVI comes from these factors, with the resulting uncertainty of about 8–16% in clear-sky conditions and about (20–40%) in cloudy conditions [18].

2.5. Techniques to Select Clear-Sky Condition

In this work, the "all-sky UV index" from OMI at noon and overpass time was used. The UV index at overpass time refers to the file attribute named OPUV index from OMUVBG product level 2G. This Surface UV Irradiance Product from OMI contains gridded surface UV irradiance, dose quantities, UV index, cloud optical thickness, and LER [69]. From GOME-2, the noontime "all-sky UV index" was also used.

To only keep clear-sky days for the comparison (ground-based vs. satellite-derived UV index), two different techniques were applied to identify clear-sky conditions: the OMI Lambertian equivalent reflectivity (LER) and cloud-cover data extracted from METAR. The LER applied in this work is derived from the OMI-measured radiance (I_{360}) near 360 nm, which can be expressed as a sum of the atmospheric backscatter above a specified Lambertian surface [70]. LER is used for cloud characterization and can be obtained in the same dataset as the UV index at overpass time from OMI [62]. Only days with an LER smaller than 10% were used [41,62].

Cloud-cover data were obtained from METAR data from Natal's international airport. This METAR is available in 1 h intervals and is free to download through the REDEMET (Air Force Command Meteorology Network) Brazilian application. METAR is a regular aerodrome weather report that contains data on temperature, wind, lightning, and others,

such as cloud cover [71]. The World Meteorological Organization defines rules for the register of cloud cover that have been traditionally carried out by human observers [72,73]. Observers divide the sky into 8 regions (octas) and evaluate the regions covered by clouds to estimate the cloud cover [72]. Here, a clear sky is considered 0 octas, denoted by the acronym CAVOK ("Ceiling in Visibility OK"), and 1 to 2 octas, denoted by the acronym FEW, corresponding to less than 30% of sky coverage [73].

2.6. Statistical Analysis

All the datasets were prepared separately and scrutinized for obvious errors. The datasets were also in UTC (Coordinated Universal Time) and had the timing adjusted to the corresponding time of Natal, which is used here (UTC-2). As the cloud cover, METAR data were in hourly frequency, and the ground-based UV index series were grouped according to the hourly average for the selection of the hours corresponding to the clear-sky condition. Then, ground-based data were analyzed for diurnal and seasonal variability under all-sky and clear-sky conditions. For ground-based measurements, a percentage difference in the hourly average UV index under clear and all-sky conditions was also calculated. This aids in better understanding how the UV index fluctuates throughout the day under these differing sky conditions. The percentage difference (PDI) was calculated as in Equation (2).

$$PDI = \left(\frac{avg_{ck} - avg_{ak}}{avg_{ak}} \right) \times 100\% \quad (2)$$

where avg_{ck} is the averaged UV index value under clear-sky conditions for the specified hour and the avg_{ak} is the averaged UV index value under all-sky conditions for the specified hour. This formula determines how much the UVI under clear-sky conditions differs from that under all-sky conditions, expressed as a percentage of the UV index under all-sky conditions.

The datasets were compared at local noontime and at the overpass time (around 1:45 p.m. local time for OMI). METAR cloud-cover data was used to select clear-sky hours in the noontime datasets. To the overpass dataset, both METAR and LER were applied since LER from OMI corresponds to the overpass time (Table 3).

Table 3. Summary of the technique used to select clear sky for each dataset of comparison.

Comparison	Technique to Select Clear Sky
Ground-based noontime vs. OMI noontime	Octas 0, 1 and 2 (METAR)
Ground-based noontime vs. GOME-2 noontime	Octas 0, 1 and 2 (METAR)
Ground-based overpass vs. OMI overpass	Octas 0, 1 and 2 (METAR) LER < 10%

To compare the ground-based with satellite data, the following metrics were calculated and analyzed: the Pearson correlation coefficient (r), the coefficient of determination (the square of the Pearson correlation coefficient r^2), Mean Bias Error (MBE), Mean Absolute Error (MAE), Mean Absolute Percentage Error (MAPE), the Root Mean Square Error (RMSE), and the p-value to determine the statistical significance of the relationship between the variables.

The Pearson's coefficient (r), Equation (3), commonly used in linear regression, is a popular correlation coefficient used to measure how strong a relationship is between two variables [74]. The correlation between the two variables is quantified with a number that varies between −1 and +1 [75]. Zero means there is no correlation, whereas 1 means a complete or perfect correlation [76]. A negative r means that the variables are inversely related [76]. The r^2 (coefficient of determination) represents the proportion of variance in the dependent variable that can be explained by the independent variable [77]. The MBE is an average of algebraic errors, while the MAE is an average of the absolute errors

(Equations (4) and (5), respectively) [78]. In this work, the MBE can indicate whether the satellite-derived UV index overestimates or underestimates the ground-based measurements. The MAPE measures the average absolute error of a model as a percentage of the actual value [79]. It represents a measure of accuracy in statistics [80], expressed as Equation (6). The RMSE is a measure of the differences between calculated values (in this study, OMI and GOME-2 data) and observed values (ground-based observations). The smaller the RMSE values, the lower the residual variance [41]. This metric is calculated as in Equation (7).

$$r = \frac{\sum_{i=1}^{n}\left(S_{GND,i} - \overline{S}_{GND}\right)\left(S_{SAT,i} - \overline{S}_{SAT}\right)}{\sqrt{\left(\sum_{i=1}^{n}\left(S_{GND,i} - \overline{S}_{GND}\right)^2\right)\left(\sum_{i=1}^{n}\left(S_{SAT,i} - \overline{S}_{SAT}\right)^2\right)}} \quad (3)$$

$$MBE = \frac{1}{n}\sum_{i=1}^{n}\left(S_{SAT,i} - S_{GND,i}\right) \quad (4)$$

$$MAE = \frac{1}{n}\sum_{i=1}^{n}\left|S_{SAT,i} - S_{GND,i}\right| \quad (5)$$

$$MAPE = \frac{1}{n}\sum_{i=1}^{n}\left(100 * \frac{\left|S_{SAT,i} - S_{GND,i}\right|}{S_{GND,i}}\right) \quad (6)$$

$$RMSE = \sqrt{\frac{1}{n-1}\sum_{i=1}^{n}\left(S_{SAT,i} - S_{GND,i}\right)^2} \quad (7)$$

where S is the UV index, $\overline{S}$ is the averaged UV index, SAT is the satellite observation, GND is the ground-based observation, and n is the number of observations.

These metrics together provide a comprehensive view of the accuracy and reliability of satellite data as compared to ground-based data. It helps in identifying potential biases, understanding the strength of the relationship, and quantifying the magnitude and relative importance of the errors.

3. Results

3.1. Ground-Based Derived UV Index Time Variability

Hourly data from the ground-based UV measurements in Natal were analyzed for the period 2006–2022. Raw data are provided in Figure 2. Data gaps are evident, with the longest being between 2017 and the end of 2018. A total of 53,286 h of UV index data was collected, with the maximum reaching 16 (extreme UV index) and an average of 6.22 (high UV index level). Throughout the years, high levels of UV start at 9 a.m. going until 3 p.m., reaching extreme between 10 a.m. and 2 p.m., as expected from a typical diurnal solar UV pattern, characterized by the increase of UV index levels during the day, to a peak reached at solar noon, and the decrease during the afternoon as solar zenith angle increases again [41].

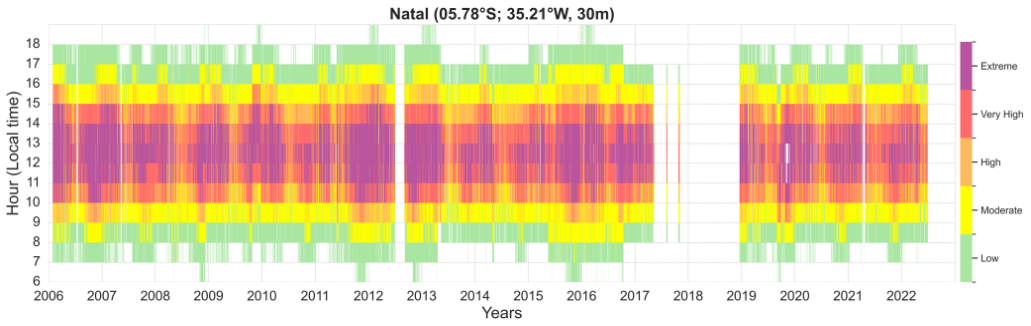

Figure 2. UV index observations as a function of day and hour per day for Natal, Brazil, from 2006 to 2022.

In this study, the comparison of ground-based and satellite-derived UV indices is made only using data from clear-sky conditions. Figure 3 shows the monthly climatological average cloud cover (in octas) for Natal for all available years between 2006 and 2022, shown as a function of time of day and month of the year, to illustrate how the cloud cover varies in Natal according to METAR cloud cover data.

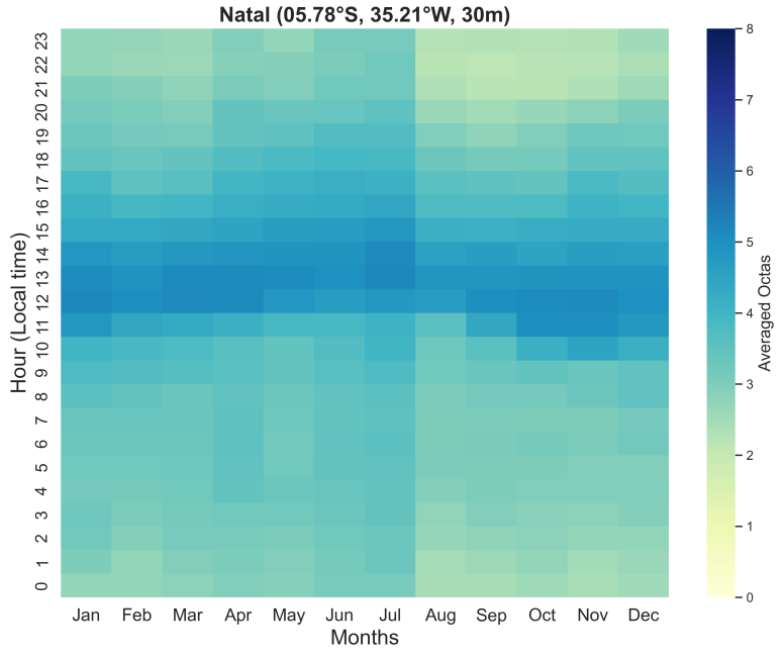

Figure 3. The monthly climatological average cloud cover (in octas) for Natal for all available years between 2006 and 2022 shown as a function of time of day and month of the year.

Around noon, there is a greater presence of cloud cover throughout the year. Clear-sky conditions prevail during night hours, as can be seen with the clear colors during these times and more hours of clear sky from August to November. These months correspond to the dry season in this region, from August to November [81]. Ref. [27] reported a similar pattern in cloud-cover variability throughout the year in their study of UV extreme events in northeast Brazil.

Figure 4a shows the percentage distribution of cloud cover for Natal for the period between 2006 and 2022, considering all day and night hours and only day hours. The clear-sky condition represents 24.18% of the day and night hours. It represents an even smaller percentage when taking into consideration only daylight hours (6 a.m. to 6 p.m.), exactly 15.21%, corresponding to 2925 h of clear-sky conditions during the days.

As indicated in Figure 4b, from 6 a.m. to 11 a.m., the averaged cloud clover indicates the predominance of scattered clouds (SCT = 3, 4 octas), while between 12 and 1 p.m., broken clouds prevail (BKN = 5, 6, 7 octas). In the afternoon, the scattered clouds prevail, but with a higher average, indicating a lower prevalence than in the morning hours. The short-term variability of the UV radiation reaching the Earth's surface is mainly controlled by changes in cloud cover [21,43,44], which mainly has an attenuating effect on the UV (20% to 70% for overcast skies) [44] but also enhancement effects manifested by increased UV irradiance at the surface compared with the equivalent clear-sky situation [21,44]. According to [45], enhancements were found to be most pronounced for large cloud cover of 5 to 7 octas (broken clouds) when the solar disk is unoccluded. This result of cloud-cover variability indicates that in Natal, around noontime, there is a greater presence of cloud cover (broken clouds), which can explain the higher UV index values registered under all-sky than under clear-sky conditions at noontime (5 and 6).

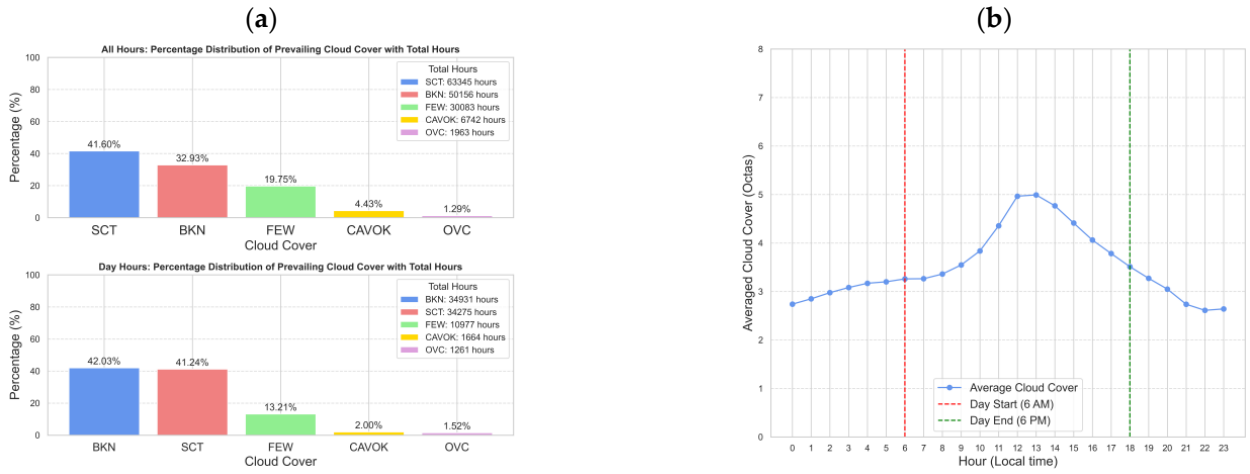

Figure 4. (**a**) Percentage distribution of cloud cover for Natal for the period between 2006 and 2022 considering all day and night hours (upper plot) and only day hours (bottom plot). (**b**) Daily climatological average cloud cover (in octas) for Natal for the period of 2006 to 2022.

In Figure 5, the monthly average ground-based UV index levels for Natal for all available years between 2006 and 2022 as a function of time of the day and month of the year under all and clear-sky conditions are presented. The UV index shows a semi-annual cycle with two maxima and a minimum in a year (Figure 5). At stations within the Tropic of Capricorn, the case of Natal, the Sun is at its peak twice a year, around the equinoxes when the Sun is directly overhead at the equator, and the stations register two annual maxima [82]. For Natal, the two peaks occurred in the summer and spring months. Similar results were reported by [48,82], and two-year maxima were also reported by [83] for Mahé. The effects of latitude on solar UV index levels are apparent, where even during austral winter months, high, very high, and extreme UV index levels were registered. Natal is located at latitude 05.78°S, where the solar zenith angle is lower throughout the year, which induces higher-intensity UV throughout the year.

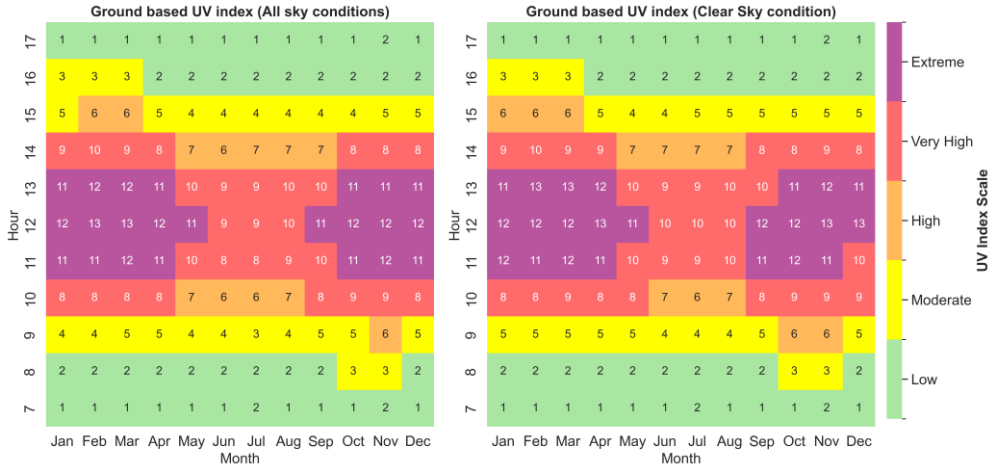

Figure 5. The monthly average ground-based UV index levels in Natal for the years between 2006 and 2022 as a function of time of day and month of the year under all and clear-sky conditions.

The UV index values were generally higher under clear-sky conditions; however, during noontime, the months of January, February, and March showed higher UV index levels under all-sky conditions than under clear-sky conditions. A similar characteristic occurred at 11 a.m. in December. The percentage difference in hourly average UV index levels between clear sky and all-sky conditions for Natal, shown in Figure 6, reinforces this result.

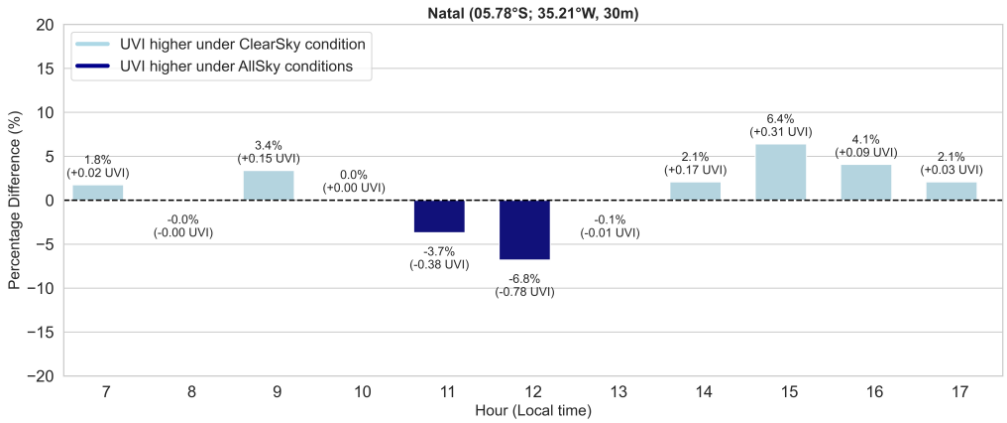

Figure 6. Percentage difference in hourly average UV index levels between clear sky and all-sky conditions for Natal for all available years between 2006 and 2022.

The UV index is higher under clear-sky conditions during the early morning and late afternoon hours. It is important to note that the difference is small, with the UV index under clear-sky conditions being at most 0.31 units higher than under all-sky conditions, peaking at 3 p.m. At noon, when the cloud average is in the broken cloud's interval (Figure 4b), the UV index under all-sky conditions is 6.8% higher than under clear-sky conditions, which means a 0.78 UV index unit higher. Ref. [82] reported an increase of 18% in the UV levels under a partially cloudy sky due to multiple reflections for the city of Maceió (9.28°S, 35.49° W, 127 m), northeast Brazil.

According to [84], surface UV can be enhanced under scattered or broken cloud conditions, occurring when the Sun is not obscured by clouds and there are clouds present elsewhere in the sky. The rainy season in Natal is concentrated between May and July [81]; however, the monthly rainfall starts to increase from December onwards [85]. Ref. [73] reported higher UV averages under all-sky conditions than under clear-sky conditions during some months (April, May, and December) of the rainy season for the city of Santarém, Northern Brazil. According to the authors, during the rainy season, factors such as the presence of cumulus or deep cirrus clouds can produce multiple scatterings, which can locally increase the UV reaching the surface [73,74].

Regarding the hourly UV index variability, the Environmental Protection Agency (EPA) informs that for the average person, low danger from the Sun's UV rays only occurs when the UV index ranges from 0 to 2. Even so, it is recommended to wear sunglasses on clear days, protect yourself with clothing, and use broad-spectrum SPF30+ sunscreen [86]. In Natal, this low-danger period only occurs until 8 in the morning and 4 in the afternoon (Figure 7). It is important to note that even during those hours, moderate levels were recorded (Figure 7).

At 9 a.m., the predominance is moderate, achieving high intensity. At 3 p.m., most of the UV is moderate, and very high levels are achieved. When the level is at most moderate, the recommendations are as follows: Stay in the shade; if outdoors, wear protective clothing, a wide-brimmed hat, and UV-blocking sunglasses; generously apply broad-spectrum SPF30+ sunscreen every 2 h, even on cloudy days and after swimming or sweating; avoid long stay over bright surfaces, like sand, water, and snow, which reflect and increase UV [86].

Between 10 a.m. and 2 p.m., extreme levels were recorded, with noon having medium and average UV index under all-sky conditions in the extreme range (UVI $\geq$ 11). Unprotected skin and eyes can have a sunburn in minutes if the UV index is 11 or more and there is no Sun protection [86]. It is recommended to avoid Sun exposure when these levels are reached and take all the recommendations recommended by [21,49]. During 5 h of the day, between 10 a.m. and 2 p.m. (UTC-2), the population in Natal can be exposed to extreme UV levels. The World Health Organization recommends Sun protection mainly between 10 a.m.

and 4 p.m. when radiation is most intense [21]. According to these results, protection is needed from 8 a.m. for those who frequent the city of Natal. Considering the hours with extreme levels, maximum protective measures need to be taken from 10 a.m. (UTC-2).

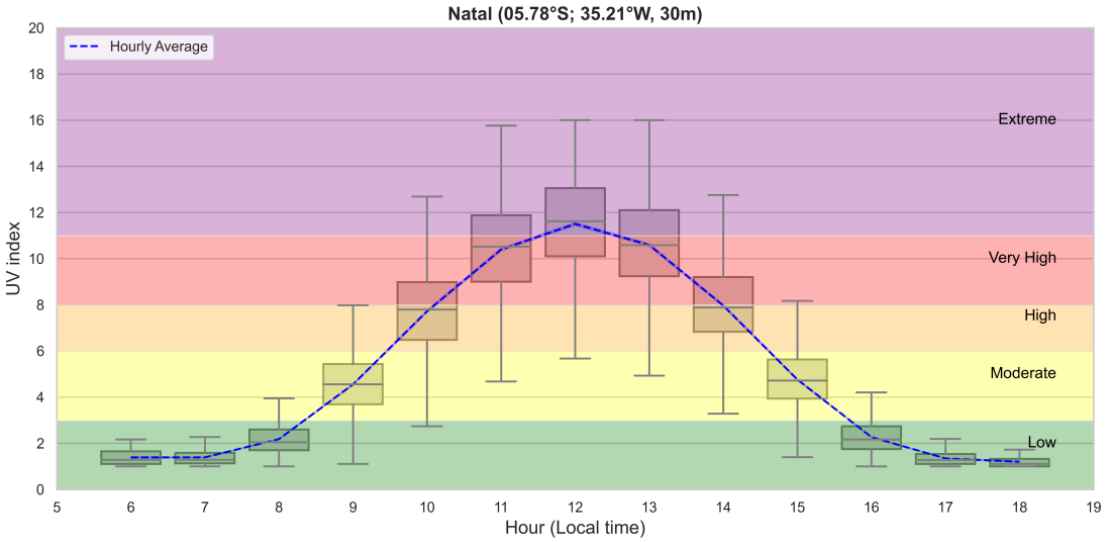

Figure 7. Hourly averaged UV index levels for Natal from 2006 to 2022.

The daily cycle of the UV index reported by [33] for the year 2008 also achieved moderate levels at 8 a.m., high at 9 a.m., and very high and extreme from 10 a.m. Similar results were reported by [31] regarding the monthly hourly UV index averages for the period of 2001–2007.

3.2. Comparison of Ground-Based vs. Satellite-Derived UV Index

Figure 8 shows the time series of the noontime and overpass time (respective to OMI) UV index from ground-based (GB) measurements in Natal under all-sky conditions. It also shows the UV index derived from OMI at noon and overpass time and from GOME-2 at noontime. The satellite, as well as the GB time series, shows a semi-annual cycle with two maxima in a year. In Natal, a daily maximum of 16 UV index has been recorded in different years. Ground-based and OMI noontime UV index presented a UV index maximum of 16, while the GOME-2 and OMI overpass reached a maximum of 14.72 and 14.80, respectively. Nevertheless, in all cases, these values represent an extreme UV index, as expected for noon and overpass time, which is around noon (approximately 1.45 p.m.).

The average UV index level from the GB at noontime was 11.50. From OMI at noontime, it was 11.41. From GOME-2 at noontime, 10.31, and according to OMI at overpass time, the average over the whole period was 8.73. In comparison with other cities around the same latitude, measurements made from 2017 to November 2020 in the city of Mahé (4.67°S, 55.53°E, 15 m a.s.l.) in Seychelles indicated UVI averages around 14 at noontime, while cities further south (Antananarivo, Anse Quitor and Saint-Denis) showed UVI averages at noontime of around 10 [83]. According to the authors, this difference is due to the difference in latitude [81]. Mahé is located at latitude 4.6.S (closer to Natal's latitude (5.78°S), and the other cities are at latitude near 20°S. Therefore, the solar zenith angle in Mahé, as in Natal, is lower throughout the year, which induces a higher-intensity UV.

Figure 9 shows the time series comparing ground-based versus satellite-derived solar UV index data from 2006 to 2022 at satellite noon and overpass time. The comparisons were performed only for clear-sky days selected with METAR, LER, and the days considered clear sky using both LER and METAR. Table 4 brings the descriptive statistics for each dataset for each comparison.

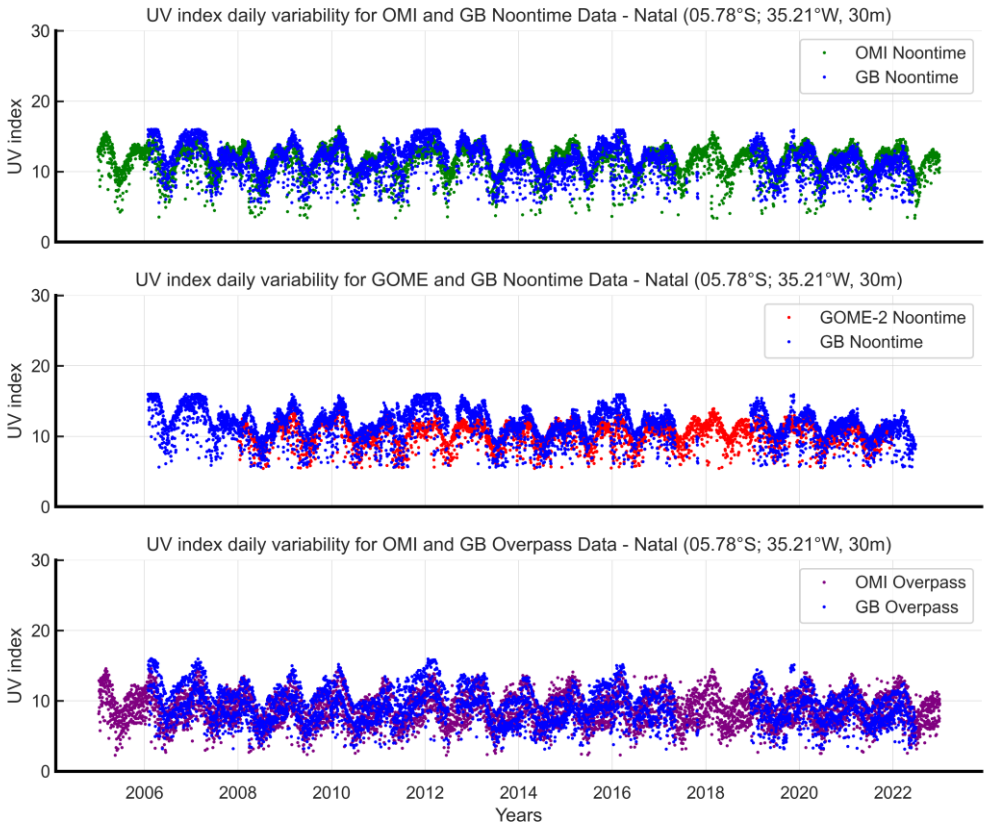

Figure 8. Daily variability of the UV index in Natal for all years of study. GB noontime refers to the ground-based data at noontime. GB overpass refers to the ground-based data at OMI overpass time.

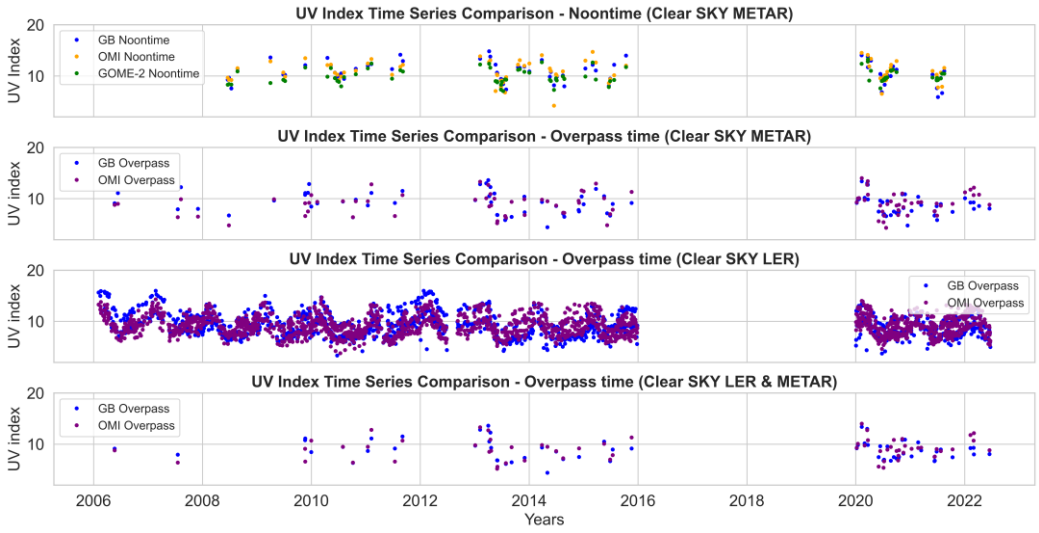

Figure 9. Time series comparing ground-based versus satellite-derived solar UV index data from 2006 to 2022 at satellite noon and overpass time. The comparisons were performed only for clear-sky days selected with METAR and LER, and the days considered clear sky using both LER and METAR.

For certain periods, a visual comparison shows large differences between the UV index levels taken from different instruments. For example, from 2008 to 2009, the differences between the noontime UVI from GB measurements and GOME-2 increased. Correlation analysis confirmed the smallest correlation between these two datasets (GB noontime vs. GOME-2 noontime) (Figure 10), where R and R^2 values ranged from a moderate positive

correlation for GB noontime vs. GOME-2 noontime to a strong positive correlation for GB noontime vs. OMI noontime.

Table 4. Summary of descriptive statistics for each time series comparison where GB Noon (ground-based UV index at local noontime) and GB OVP (ground-based UV index at local OMI overpass time); CKT (clear-sky technique) refers to the technique used to select clear-sky days.

Metrics	N	Mean	Std	Min	25%/75%	50%	Max	CKT
GB Noon	109	10.75	1.89	5.86	9.65/12.08	10.46	14.81	METAR
OMI Noon	109	10.81	1.92	4.18	9.54/12.20	10.65	14.71	METAR
GOME-2 Noon	109	9.96	1.42	7.06	9.0/11.13	9.57	13.24	METAR
GB OVP	138	9.08	2.08	4.15	7.48/10.41	9.05	15.12	METAR
OMI OVP	138	8.96	2.09	4.31	7.24/10.64	9.05	14.01	METAR
GB OVP	1928	9.14	2.18	3.16	7.46/10.53	8.95	15.96	LER
OMI OVP	1928	9.24	1.93	3.80	7.79/10.55	9.10	14.70	LER
GB OVP	95	8.98	1.98	4.15	7.44/10.26	8.96	15.12	Both
OMI OVP	95	9.06	1.98	5.20	7.55/10.69	9.06	14.01	Both

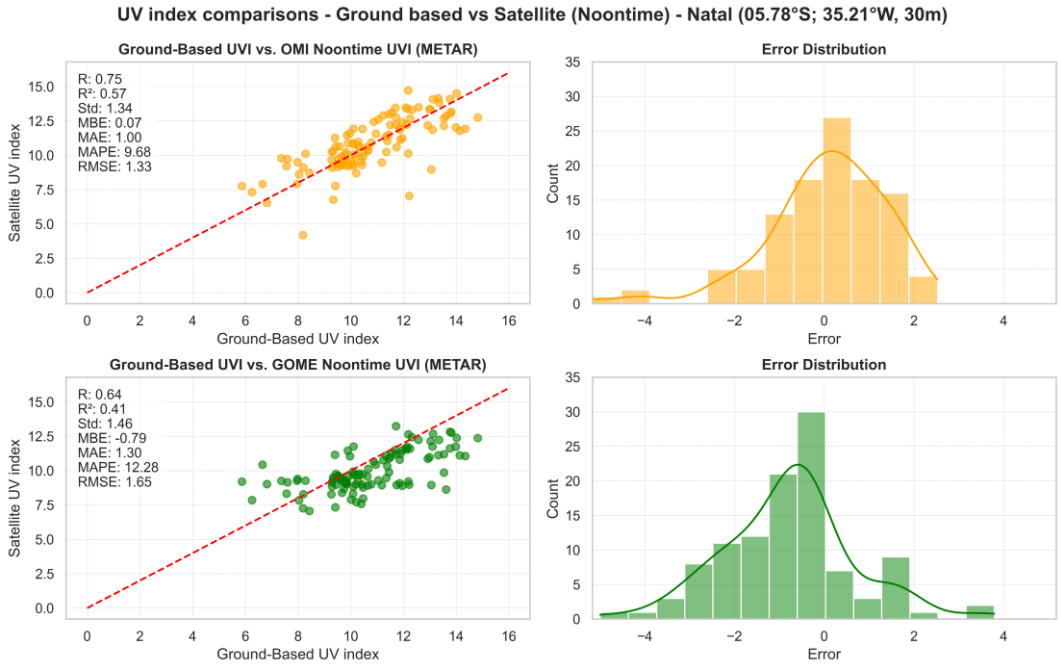

Figure 10. Correlation between ground-based UV index and satellite-derived UV index data (OMI, GOME-2) from 2008 to 2022 for Natal at local noontime and under clear-sky conditions selected with METAR. The Red dashed line represents the line of perfect agreement (y = x). *p*values : 2.68×10^{-21}, 4.48×10^{-06}. The first p − value refers to GB vs. OMI (noontime) and the second to GB vs. GOME-2 (noontime).

GB overpass vs. OMI overpass, in all scenarios (clear-sky LER, clear-sky METAR, and clear-sky both), also presented moderate to strong positive correlation (0.62, 0.69, and 0.70, respectively). Ref. [41] reported a positive moderate correlation between ground−based versus OMI−derived UV index for the city of Pretoria (25.73°S, 28.18°E, 1330 m from 1994 to May 2003 and 25.81°S, 28.49°E, 1228 m from May 2003 to 2015) in South Africa.

The positive MBE (Figure 10) suggests that, on average, UVI derived from OMI at noontime overestimates the GB UVI by 0.07 units in Natal. From the comparison of GB noontime vs. GOME-2 noontime, the negative MBE suggests that, on average, the UVI derived from GOME-2 at noontime underestimates the GB UVI by −0.79 units. For the overpass time (Figure 11), the negative MBE suggests that on average, UVI derived from

OMI overpass (METAR) also underestimates the GB UVI by −0.12 units, while when using LER to select clear-sky days, the MBE suggests that on average UVI derived from OMI at overpass time overestimates the GB UVI by 0.10 units. When using both techniques, it has the smallest absolute MBE of the three, indicating it is the least biased.

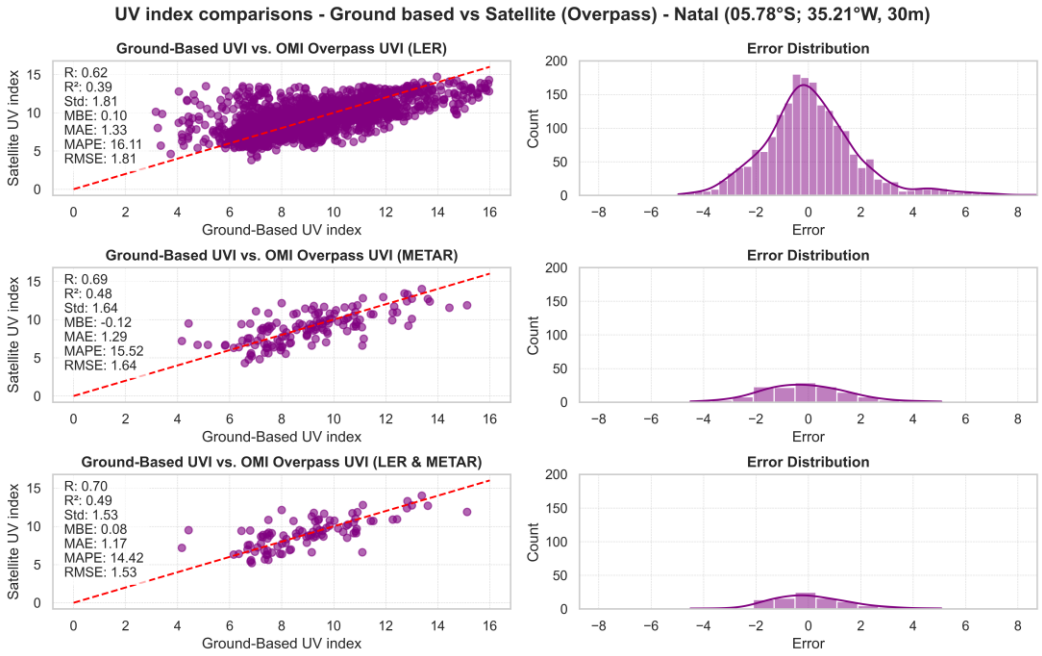

Figure 11. Correlation between ground-based UV index and satellite-derived UV index data (OMI) from 2006 to 2022 for Natal at overpass time and under clear-sky conditions selected with LER, METAR, and hour considered clear sky using both techniques (LER, METAR). p values : 1.80×10^{-206}, 3.93×10^{-21}, 2.51×10^{-15}. The first $p-$value refers to GB vs. OMI (overpass−LER), the second to GB vs. OMI (overpass−METAR), and the third to GB vs. OMI (overpass−LER and METAR).

According to [87], the validation of UV index retrieved from OMI at noontime against ground-based measurements at different climates in Egypt performed in all-sky conditions in the period 2012–2017 at three sites: Aswan (23.97°N, 32.78°E, 192.5 m, Pyranometer), Cairo (30.08°N, 31.28°E, 34.4 m, Pyranometer) and Matruh 31.33°N, 27.22°E, 25 m, Brewer MK II) showed that OMI overestimates ground-based observations in all seasons at all stations with annual mean bias of 0.52, 0.68 and 1.02 to Aswan, Cairo and Matruh, respectively.

Ref. [88] examined the OMI UV performance in different cloudiness conditions using ground-based observations in Jokioinen (60.8°N, 23.5°E) and Sodankylä (67.3°N, 26.6°E) for the years 2005 to 2011 at the time of satellite overpass. They reported that for both Jokioinen and Sodankylä, OMI UV overestimates the surface UV index with a mean bias of 0.50 for Jokioinen and 0.26 for Sodankylä under clear-sky conditions. Ref. [3] found that at Irene (25.91°S, 28.21°E, 1523 m), De Aar (30.67°S, 23.99°E, 1284 m) and Upington (28.48°S, 21.12°E, 848 m), the GOME-2 data underestimated surface UVA measurements with MBE of −5.5, −11.2 and −12.8 at Irene, De Aar and Upington, respectively, under clear-sky conditions.

The MAE of 1 means that, on average, the absolute difference between the UVI derived from OMI and the GB at noontime is 1, and for GOME-2 is 1.30. The MAE at overpass time, using the three techniques, is higher than the MAE from OMI noontime, indicating that the OMI overpass UVI has the largest average deviation from the GB UVI, even though the difference is quite small between all the datasets. The MAPE of 9.68 implies that the UVI derived from OMI deviates by about 9.68% on average from the GB UVI at noontime. The largest deviation occurred between the OMI and GB overpass time when using the LER technique, with a deviation of 16.11%.

Ref. [41] reported that the MAPE between OMI and ground-based index at overpass time using LER were 27% for Pretoria (25.73°S, 28.18°E, 1330 m, 1994 to May 2003), 28% for Durban (29.97°S, 31.00°E, 9 m, 1994 to May 2010) and 46% for De Aar (30.67°S, 23.99°E 1286 m 2002 to 2015). Comparisons between ground-based and OMI-derived UV index at noontime showed annual MAPE of 10.6% for Aswan (23.97°N, 32.78°E, 192.5 m, Pyranometer), 17.3% for Cairo (30.08°N, 31.28°E, 34.4 m, Pyranometer) and 26.0% for Maltruh (31.33°N, 27.22°E, 25 m, Brewer MK II) for the period between 2012 and 2017, under all-sky conditions [87]. This means that even if the MAPE at overpass time in this work is higher than at noontime, still the agreement is better than the agreement between OMI overpass and the ground-based measurements made in Cairo and Maltruh cities in Egypt by [87] and in Pretoria, Durban, and De Aar in South Africa [41].

The comparison between GB and OMI at noontime has the lowest RMSE (1.33) of all comparisons. This suggests that the OMI noontime estimations are in closer agreement with the GB non-noontime measurements compared to the GOME-2 noontime and OMI overpass estimations. Nevertheless, the difference between the metrics results is quite small between the datasets, showing that satellite UV index measurements have a good agreement with the ground-based measurements, as indicated by the moderate to high correlation coefficients and the clustering of points near the red line in the scatter plots. Another indicator of this good agreement is the error distribution plots. These plots reveal that most errors cluster around zero. Notably, the GOME-2 noontime and OMI overpass (METAR) data are slightly skewed to the left, aligning with the negative Mean Bias Error (MBE) and reinforcing the slight underestimation observed.

4. Discussion

The Davis 6490 UV sensor used to monitor UV levels in Natal has an accuracy of ±5%, with a drift of up to ±2% per year [57]. The most notable error sources for this instrument include troubleshooting due to cable connections, plugs not firmly seated, and lack of calibration in the frequency recommended in the user manual [57]. For the first time, the entire dataset from 2006 to 2022 of UV index levels in Natal monitored with the Davis Sensor 6490 has been analyzed for diurnal and seasonal variability under all and clear-sky conditions. Furthermore, the main objective of this study was to conduct a comparative analysis of ground-based and satellite-derived UV index levels from OMI and GOME-2 in Natal, Brazil, under clear-sky conditions, to assess the reliability of different satellite-derived UV index data for this site, should these data be used for long-term trend analysis, or the monitoring of solar UV exposure risk and possible impacts to the environment.

Regarding the UV time variability in Natal, the UV index showed a semi-annual cycle with two maxima in a year, during austral summer and spring, with smaller UV index levels during austral winter. The less-intense levels during austral winter, around noon, continue to be very high levels on the UV index scale. These characteristics agree with what is expected for a city at the location of Natal, at latitude 05.78°S, where the solar zenith angle is lower throughout the year, inducing higher-intensity UV throughout the year. Also, since Natal is within the Tropic of Capricorn, the Sun is at its peak twice a year, around the equinoxes when the Sun is directly overhead at the equator, with the stations recording two annual maxima [40].

Another important characteristic is that in Natal, around noon, there is a greater presence of cloud cover throughout the year (average in the broken clouds interval). Clear-sky conditions prevail during night hours, and there are more hours of clear sky between August and November, the dry period in the region. The clear-sky condition represents only 15.21% of daylight hours. This pattern of cloud-cover variability can explain the higher UV index values registered under all-sky than under clear-sky conditions at 11 a.m. and 12 p.m. since it is already indicated in the literature that partially cloudy skies, under scattered or broken clouds, can produce multiple scatterings that can increase locally UV levels at the surface, reaching levels higher than under clear skies [17,46,74].

These results indicate that in Natal, even during clear or all-sky conditions, the UV index is generally high. Between 10 a.m. and 2 p.m., the population in Natal can be exposed to extreme UV levels. Therefore, protection is needed from 8 a.m. for those who frequent the city of Natal. Considering the hours with extreme levels, maximum protective measures need to be taken from 10 a.m. It is important to note that this study uses UTC-2, according to the latitude at which Natal is located, but the inhabitants of Natal follow the UTC of the capital of Brazil, Brasilia (UTC-3). This means that from 7 a.m., anyone visiting or living in Natal must protect themselves adequately from the UV radiation, with maximum protective measures needed from 9 a.m. onwards if following UTC-3.

Regarding the comparisons between ground-based and satellite-derived UV index, OMI UVI at the overpass and noontime presents less bias than GOME-2 UVI. While OMI mainly overestimates the UV index levels in comparison with ground-based measurements, GOME-2 underestimates it. UV products derived from OMI are known to overestimate ground-based measurements [60–62,87,88]. Part of the positive bias between OMI UVI and ground-based UVI is due to absorbing aerosols [18,62]. It is important to emphasize that this is not a statement particular about the Natal, although the inaccurate description of the absorbing aerosols is a possible explanation for the observed discrepancies. Other factors of uncertainty are clear-sky irradiance modeling (depending on ozone surface albedo), the cloud–aerosol correction factor, and satellite overpass occurring at a time significantly different from local noon [18]. In Natal, the satellite overpass of OMI is about 13:45 $\pm$ 15 min LT), not too different from the noontime, 12 p.m. While the overpass time of the GOME-2 (09:30 a.m. LT) is more distant from noontime. Another factor of uncertainty on GOME-2 UV products is also the climatology of aerosols and surface albedo used in the algorithm, which was not determined from observations [3].

Through this study, it was possible to identify that the technique used to select a clear sky also affects the statistical comparison metrics. For example, regarding the difference between the techniques used to identify clear-sky conditions, the LER method identified a significantly larger number of clear-sky days (1928 days) compared to the METAR method (138 days) at overpass time. This significant difference suggests that the LER method could have more flexible criteria for defining "clear-sky" conditions, potentially including days with more cloud cover compared to what METAR considers as clear-sky. The difference in the number of clear-sky days identified confirms that these two methods have vastly different criteria for identifying clear-sky days. METAR seems to be more conservative than LER. The difference between the METAR alone and the combined METAR and LER (43 days) indicates that there are days that METAR identifies as clear-sky days but are not considered clear-sky days when using the combined approach. This could potentially be days with minor cloud cover that METAR considers, but LER does not. These differences highlight the importance of understanding the specific criteria each method uses to identify clear-sky days and suggest that a careful selection or combination of methods might be necessary to obtain the most accurate representation of clear-sky days for each specific study or application.

Another point is that the negative MBE values associated with the METAR technique indicate that the satellite-derived UV index levels are, on average, lower than the ground-based UV index measurements. This discrepancy could potentially be due to the METAR data indicating clear skies, while the satellite data identifies these days as not entirely clear, estimating lower UVI values. The METAR data are usually based on observations at airports and represent local clear-sky conditions more accurately than satellite data, which captures a larger area. For satellite observations, the variation introduced by clouds is spatially averaged over the area of the pixel [89]; therefore, the satellite data might be noticing atmospheric or cloud-cover variations over a broader region that are not captured in the localized METAR. Implementing sky cameras installed near the UV sensor could reduce uncertainties associated with the technique used to determine clear-sky conditions. These cameras would provide clear images of the sky, helping to determine the

actual sky conditions more accurately, thus potentially reducing uncertainty related to the sky condition.

Overall, metrics such as MAE, MAPE, and RMSE indicate that differences between the satellite and ground-based measurements are generally low. Together with the moderate and strong correlation coefficients, the clustering of points near the red line in the scatter plots, and the error distribution plots clustered around zero, the analysis indicates that the two satellite sources (OMI noontime and overpass) and GOME-2 noontime are a reliable source for UV index data, showing good agreement with ground-based measurements.

5. Conclusions

The main aim of this paper was to conduct a comparative analysis between the ground-based measured UV index levels in Natal, Brazil, and the satellite-derived UV index from OMI and GOME-2. The comparison reported here was carried out using UV index levels under clear-sky conditions. The hours of clear sky were selected using cloud-cover data from METAR, using LER, and applying both techniques together. Furthermore, in this paper, an analysis of the diurnal and seasonal variability of the UV index under all clear-sky conditions in Natal was also reported.

For all the time series, the UV index showed an annual cycle with two maxima in a year, during austral summer and spring, with smaller UV index levels during austral winter. The less-intense levels during austral winter, around noon, continue to be very high levels on the UV index scale. In Natal, a daily maximum of 16 UV indexes were recorded in different years in the ground-based and OMI noontime time series. The UV index was derived from GOME-2, and the OMI overpass reached less than 15. Nevertheless, in all cases, these values represent an extreme UV index.

There has been a greater presence of cloud cover around noontime in Natal all over the years. Clear-sky conditions prevail during night hours, with hours of clear sky representing only 15.21% of daylight. There are more hours of clear sky between August and November, the dry period in the region. The UV index under all-sky is higher than under clear-sky conditions from 11 a.m. to noon, hours when the averaged cloud cover indicates a greater presence of broken clouds, suggesting the influence of cloud cover in enhancing the ground-based UV index levels under partially cloudy skies.

In Natal, the low-danger period of exposure to UV rays only occurs until 8 a.m. and from 4 p.m. onwards. However, even during those hours, moderate levels were recorded. Therefore, protection is needed from 8 a.m. for those who frequent the city of Natal. Between 10 a.m. and 2 p.m., the population in Natal is exposed to extreme UV levels. Considering the hours with extreme levels, maximum protective measures need to be taken from 10 a.m., considering UTC-2. When following UTC-3, these recommendations should be followed 1 h in advance.

The differences between the techniques used to identify clear-sky conditions highlight the importance of understanding the specific criteria each method uses to identify clear-sky days and suggest that a careful selection or combination of methods might be necessary to obtain the most accurate representation of clear-sky days for each specific study.

The errors between the satellite and ground-based measurements are generally low, with the analysis indicating that the two satellite sources (OMI noontime and overpass) and GOME-2 noontime are reliable sources for UV index data, showing good agreement with ground-based measurements. OMI UVI at noon and overpass time are less biased than GOME-2 noontime UVI.

This study differs from previous studies and contributes to the scientific understanding of UV radiation levels using unpublished UV index data from a ground-based station in a city located near the equator, in South America's tropical region, where until now, there has been relatively limited research focusing on this field of study. With the reliability of these satellite data accessed for Natal, we will study the trends of the UV index in this tropical Brazilian site in future works.

Author Contributions: Conceptualization, G.C.G.d.R. and H.B.; methodology, G.C.G.d.R.; software, G.C.G.d.R.; validation, G.C.G.d.R., H.B., K.L. and F.R.d.S.; formal analysis, G.C.G.d.R. and M.A.G.d.R.; investigation, G.C.G.d.R.; resources, R.S., L.V.P., T.P., D.K.P. and F.R.d.S.; data curation, G.C.G.d.R. and M.A.G.d.R.; writing—original draft preparation, G.C.G.d.R.; writing—review and editing, G.C.G.d.R.; visualization, G.C.G.d.R., H.B., M.A.G.d.R. and L.V.P.; supervision, R.S., L.V.P., H.B. and T.P.; project administration, G.C.G.d.R.; funding acquisition, G.C.G.d.R., D.K.P., L.V.P., R.S. and T.P. All authors have read and agreed to the published version of the manuscript.

Funding: This research was funded by FAPESPA (Amazon Foundation for the Support of Studies and Research), by CAPES (Coordination for the Improvement of Higher Education Personnel), a foundation linked to the Brazilian Ministry of Education, CAPES project number 88887.130199/2017—01, COFECUB (French Evaluation Committee of the University and Scientific Cooperation with Brazil) and by the French Government under the 2023 Campus France project of cotutelle cost-sharing doctoral scholarships. The APC was funded by Universidade Federal do Oeste do Pará.

Data Availability Statement: Data are available on request from G.C.G.d.R.

Acknowledgments: We acknowledge the support and funding of this work by the FAPESPA for the PhD scholarship in the Post Graduate Program in Society Nature and Development. To CAPES (Coordination for the Improvement of Higher Education Personnel) and COFECUB (French Evaluation Committee of the University and Scientific Cooperation with Brazil) for the sandwich PhD scholarship awarded to the MESO project (Modeling and Prediction of the Secondary Effects of the Antarctic Ozone hole). To the French Government, Campus France, LACy (UMR 8105 CNRS, Météo-France), and the University of Réunion.

Conflicts of Interest: The authors declare no conflicts of interest.

References

1. Cadet, J.-M.; Bencherif, H.; Cadet, N.; Lamy, K.; Portafaix, T.; Belus, M.; Brogniez, C.; Auriol, F.; Metzger, J.-M.; Wright, C.Y. Solar UV Radiation in the Tropics: Human Exposure at Reunion Island (21° S, 55° E) during Summer Outdoor Activities. *Int. J. Environ. Res. Public Health* **2020**, *17*, 8105. [CrossRef]
2. Diffey, B.L. Solar Ultraviolet Radiation Effects on Biological Systems. *Phys. Med. Biol.* **1991**, *36*, 299–328. [CrossRef] [PubMed]
3. Du Preez, D.J.; Parisi, A.V.; Millar, D.A.; Benchérif, H.; Wright, C.Y. Comparison of GOME-2 UVA Satellite Data to Ground-Based UVA Measurements in South Africa. *Photochem. Photobiol.* **2020**, *96*, 1342–1349. [CrossRef]
4. United Nations Environment Programme. *Environmental Effects of Stratospheric Ozone Depletion, UV Radiation, and Interactions with Climate Change: 2022 Assessment Report*; UNEP Ozone Secretariat: Nairobi, Kenya, 2023. Available online: https://ozone.unep.org/system/files/documents/EEAP-2022-Assessment-Report-May2023.pdf (accessed on 27 October 2023).
5. Lucas, R.M.; Yazar, S.; Young, A.R.; Norval, M.; de Gruijl, F.R.; Takizawa, Y.; Rhodes, L.E.; Sinclair, C.A.; Neale, R.E. Human Health in Relation to Exposure to Solar Ultraviolet Radiation under Changing Stratospheric Ozone and Climate. *Photochem. Photobiol. Sci.* **2019**, *18*, 641–680. [CrossRef]
6. Lucas, R.M.; Byrne, S.N.; Correale, J.; Ilschner, S.; Hart, P.H. Ultraviolet Radiation, Vitamin D and Multiple Sclerosis. *Neurodegener. Dis. Manag.* **2015**, *5*, 413–424. [CrossRef]
7. Lindqvist, P.G.; Epstein, E.; Nielsen, K.; Landin-Olsson, M.; Ingvar, C.; Olsson, H. Avoidance of Sun Exposure as a Risk Factor for Major Causes of Death: A Competing Risk Analysis of the Melanoma in Southern Sweden Cohort. *J. Intern. Med.* **2016**, *280*, 375–387. [CrossRef]
8. Lindqvist, P.G.; Landin-Olsson, M. The Relationship between Sun Exposure and All-Cause Mortality. *Photochem. Photobiol. Sci.* **2017**, *16*, 354–361. [CrossRef]
9. Olsen, C.M.; Wilson, L.F.; Green, A.C.; Bain, C.J.; Fritschi, L.; Neale, R.E.; Whiteman, D.C. Cancers in Australia Attributable to Exposure to Solar Ultraviolet Radiation and Prevented by Regular Sunscreen Use. *Aust. N.Z. J. Public Health* **2015**, *39*, 471–476. [CrossRef]
10. Yousif, E.; Haddad, R. Photodegradation and Photostabilization of Polymers, Especially Polystyrene: Review. *SpringerPlus* **2013**, *2*, 398. [CrossRef]
11. Andrady, A.L.; Heikkilä, A.M.; Pandey, K.K.; Bruckman, L.S.; White, C.C.; Zhu, M.; Zhu, L. Effects of UV Radiation on Natural and Synthetic Materials. *Photochem. Photobiol. Sci.* **2023**, *22*, 1177–1202. [CrossRef]
12. Bornman, J.F.; Barnes, P.W.; Robinson, S.A.; Ballaré, C.L.; Flint, S.D.; Caldwell, M.M. Solar Ultraviolet Radiation and Ozone Depletion-Driven Climate Change: Effects on Terrestrial Ecosystems. *Photochem. Photobiol. Sci.* **2015**, *14*, 88–107. [CrossRef] [PubMed]
13. Ballaré, C.L.; Caldwell, M.M.; Flint, S.D.; Robinson, S.A.; Bornman, J.F. Effects of Solar Ultraviolet Radiation on Terrestrial Ecosystems. Patterns, Mechanisms, and Interactions with Climate Change. *Photochem. Photobiol. Sci.* **2011**, *10*, 226. [CrossRef]
14. Bancroft, B.A.; Baker, N.J.; Blaustein, A.R. Effects of UVB Radiation on Marine and Freshwater Organisms: A Synthesis through Meta-Analysis. *Ecol. Lett.* **2007**, *10*, 332–345. [CrossRef]

15. Sulzberger, B.; Austin, A.T.; Cory, R.M.; Zepp, R.G.; Paul, N.D. Solar UV Radiation in a Changing World: Roles of Cryosphere—Land—Water—Atmosphere Interfaces in Global Biogeochemical Cycles. *Photochem. Photobiol. Sci.* **2019**, *18*, 747–774. [CrossRef] [PubMed]
16. Erickson III, D.J.; Sulzberger, B.; Zepp, R.G.; Austin, A.T. Effects of Stratospheric Ozone Depletion, Solar UV Radiation, and Climate Change on Biogeochemical Cycling: Interactions and Feedbacks. *Photochem. Photobiol. Sci. S* **2015**, *14*, 127–148. [CrossRef]
17. Porfirio, A.C.S.; De Souza, J.L.; Lyra, G.B.; Maringolo Lemes, M.A. An Assessment of the Global UV Solar Radiation under Various Sky Conditions in Maceió-Northeastern Brazil. *Energy* **2012**, *44*, 584–592. [CrossRef]
18. Brogniez, C.; Auriol, F.; Deroo, C.; Arola, A.; Kujanpää, J.; Sauvage, B.; Kalakoski, N.; Pitkänen, M.R.A.; Catalfamo, M.; Metzger, J.-M.; et al. Validation of Satellite-Based Noontime UVI with NDACC Ground-Based Instruments: Influence of Topography, Environment and Satellite Overpass Time. *Atmos. Chem. Phys.* **2016**, *16*, 15049–15074. [CrossRef]
19. Vitt, R.; Laschewski, G.; Bais, A.; Diémoz, H.; Fountoulakis, I.; Siani, A.-M.; Matzarakis, A. UV-Index Climatology for Europe Based on Satellite Data. *Atmosphere* **2020**, *11*, 727. [CrossRef]
20. Bernhard, G.H.; Bais, A.F.; Aucamp, P.J.; Klekociuk, A.R.; Liley, B.; McKenzie, R. Stratospheric Ozone, UV Radiation, and Climate Interactions. *Photochem. Photobiol. Sci.* **2023**, *22*, 937–989. [CrossRef]
21. World Health Organization. Solar Ultraviolet Radiation: Global Burden of Disease from Solar Ultraviolet Radiation. Available online: https://www.who.int/publications/i/item/9241594403 (accessed on 13 October 2023).
22. de Paula Corrêa, M. Solar Ultraviolet Radiation: Properties, Characteristics and Amounts Observed in Brazil and South America. *An. Bras. Dermatol.* **2015**, *90*, 297–313. [CrossRef]
23. Suarez Salas, L.F.; Flores Rojas, J.L.; Pereira Filho, A.J.; Karam, H.A. Ultraviolet Solar Radiation in the Tropical Central Andes (12.0° S). *Photochem. Photobiol. Sci.* **2017**, *16*, 954–971. [CrossRef]
24. Estupiñán, J.G.; Raman, S.; Crescenti, G.H.; Streicher, J.J.; Barnard, W.F. Effects of Clouds and Haze on UV-B Radiation. *J. Geophys. Res. Atmos.* **1996**, *101*, 16807–16816. [CrossRef]
25. World Health Organization; World Meteorological Organization; United Nations Environment Programme & International Commission on Non-Ionizing Radiation Protection. Global Solar UV Index: A Practical Guide. Available online: https://apps.who.int/iris/handle/10665/42459 (accessed on 13 October 2023).
26. Bilbao, J.; de Migue, A. Erythemal Solar Irradiance, UVER, and UV Index from Ground-Based Data in Central Spain. *Appl. Sci.* **2020**, *10*, 6589. [CrossRef]
27. Lopo, A.B.; Helena, M.; Sérgio Lúcio, P.; Pinheiro, M. UV Extreme Events in Northeast Brazil. *Ciência E Nat.* **2014**, *36*, 482–490. [CrossRef]
28. Schalka, S.; Steiner, D.; Ravelli, F.N.; Steiner, T.; Terena, A.C.; Marçon, C.R.; Ayres, E.L.; Addor, F.A.S.; Miot, H.A.; Ponzio, H.; et al. Brazilian Consensus on Photoprotection. *An. Bras. Dermatol.* **2014**, *89*, 1–74. [CrossRef]
29. Herman, J.R.; DeLand, M.T.; Huang, L.; Labow, G.J.; Larko, D.; Lloyd, S.A.; Mao, J.; Qin, W.; Weaver, C.J. A Net Decrease in the Earth's Cloud, Aerosol, and Surface 340 Nm Reflectivity during the Past 33 Yr (1979–2011). *Atmos. Chem. Phys.* **2013**, *13*, 8505–8524. [CrossRef]
30. Augusto, J.; Ottaiano, A.; Pereira De Ávila, M.; Caixeta, C.; Alexandre, U.; Taleb, C. As Condições de Saúde Ocular No Brasil 2019. 2008. Available online: https://www.cbo.com.br/novo/publicacoes/condicoes_saude_ocular_brasil2019.pdf (accessed on 5 September 2023).
31. da Silva, F.R.; de Oliveira, H.S.M.; Marinho, G.S. Variação Do Índice de Radiação Solar Ultravioleta Em Natal—RN Entre 2001 E 2007. In Proceedings of the Congresso Brasileiro de Energia Solar-CBENS, Florianópoli, Brazil, 18–21 November 2008. Available online: https://anaiscbens.emnuvens.com.br/cbens/article/view/1336/1329 (accessed on 2 September 2023).
32. Marinho, G.S.; da Silva, F.R. Aspectos Da Radiação Ultravioleta Solar Em Natal—RN–BRASIL. *Soc. E Territ.* **2013**, *25*, 29–41. Available online: https://periodicos.ufrn.br/sociedadeeterritorio/article/view/3522 (accessed on 3 September 2023).
33. Lopo, A.B.; Spyrides, M.H.C.; Lucio, P.S.; Sigró, J. Radiação Ultravioleta, Ozônо E Total Aerossóis Na Cidade de Natal—RN. *HOLOS* **2013**, *6*, 3–21. [CrossRef]
34. Cadet, B.; Goldfarb, L.; Faduilhe, D.; Giraud, S.; Keckhut, P.; Réchou, A. A Sub-Tropical Cirrus Clouds Climatology from Reunion Island (21°S, 55°E) Lidar Data Set. *Geophys. Res. Lett.* **2003**, *30*. [CrossRef]
35. Fountoulakis, I.; Diémoz, H.; Siani, A.-M.; Laschewski, G.; Filippa, G.; Arola, A.; Bais, A.F.; De Backer, H.; Lakkala, K.; Webb, A.R.; et al. Solar UV Irradiance in a Changing Climate: Trends in Europe and the Significance of Spectral Monitoring in Italy. *Environments* **2020**, *7*, 1. [CrossRef]
36. United Nations Environment Programme (UNEP). Environmental Effects and Interactions of Stratospheric Ozone Depletion, UV Radiation, and Climate Change; 2018 Assessment Report; Nairobi, Kenya. Available online: https://ozone.unep.org/science/assessment/eeap (accessed on 23 September 2023).
37. Parra, R.; Cadena, E.; Flores, C. Maximum UV Index Records (2010–2014) in Quito (Ecuador) and Its Trend Inferred from Remote Sensing Data (1979–2018). *Atmosphere* **2019**, *10*, 787. [CrossRef]
38. Fontana, F.; Lugrin, D.; Seiz, G.; Meier, M.; Foppa, N. Intercomparison of Satellite- and Ground-Based Cloud Fraction over Switzerland (2000–2012). *Atmos. Res.* **2013**, *128*, 1–12. [CrossRef]
39. Silva, A.A.; Pereira, M. Ground-Based Measurements of Local Cloud Cover. *Meteorol. Atmos. Phys.* **2013**, *120*, 201–212. [CrossRef]
40. Damiani, A.; Cordero, R.R.; Cabrera, S.; Laurenza, M.; Rafanelli, C. Cloud Cover and UV Index Estimates in Chile from Satellite-Derived and Ground-Based Data. *Atmos. Res.* **2014**, *138*, 139–151. [CrossRef]

41. Cadet, J.-M.; Bencherif, H.; Portafaix, T.; Lamy, K.; Ncongwane, K.; Coetzee, G.J.R.; Wright, C.Y. Comparison of Ground-Based and Satellite-Derived Solar UV Index Levels at Six South African Sites. *Int. J. Environ. Res. Public Health* **2017**, *14*, 1384. [CrossRef] [PubMed]
42. González-Rodríguez, L.; Rodríguez-López, L.; Jiménez, J.; Luis, J.; García, W.; Duran-Llacer, I.; Pereira, A.; Barja, B. Spatio-Temporal Estimations of Ultraviolet Erythemal Radiation in Central Chile. *Air Qual. Atmos. Health* **2022**, *15*, 837–852. [CrossRef]
43. Kosmopoulos, P.G.; Kazadzis, S.; Schmalwieser, A.W.; Raptis, P.I.; Papachristopoulou, K.; Fountoulakis, I.; Masoom, A.; Bais, A.F.; Bilbao, J.; Blumthaler, M.; et al. Real-Time UV Index Retrieval in Europe Using Earth Observation-Based Techniques: System Description and Quality Assessment. *Atmos. Meas. Tech.* **2021**, *14*, 5657–5699. [CrossRef]
44. Bernhard, G.; Seckmeyer, G. Uncertainty of Measurements of Spectral Solar UV Irradiance. *J. Geophys. Res. Atmos.* **1999**, *104*, 14321–14345. [CrossRef]
45. Zhang, H.; Wang, J.; Castro García, L.; Zeng, J.; Dennhardt, C.; Liu, Y.; Krotkov, N.A. Surface Erythemal UV Irradiance in the Continental United States Derived from Ground-Based and OMI Observations: Quality Assessment, Trend Analysis and Sampling Issues. *Atmos. Chem. Phys.* **2019**, *19*, 2165–2181. [CrossRef]
46. du Preez, D.J.; Bencherif, H.; Portafaix, T.; Lamy, K.; Wright, C.Y. Solar Ultraviolet Radiation in Pretoria and Its Relations to Aerosols and Tropospheric Ozone during the Biomass Burning Season. *Atmos.* **2021**, *12*, 132. [CrossRef]
47. Kerr, J.B.; Fioletov, V.E. Surface Ultraviolet Radiation. *Atmos.-Ocean* **2008**, *46*, 159–184. [CrossRef]
48. Kirchhoff, V.W.J.H.; Echer, E.; Leme, N.P.; Silva, A.A. A Variação Sazonal Da Radiação Ultravioleta Solar Biologicamente Ativa. *Rev. Bras. Geofísica* **2000**, *18*, 63–74. [CrossRef]
49. Instituto Brasileiro de Geografia Estatística (IBGE). Estimativas Da População Residente Para Os Municípios E Para as Unidades Da Federação | IBGE. Available online: https://www.ibge.gov.br/estatisticas/sociais/populacao/9103-estimativas-de-populacao.html (accessed on 15 September 2023).
50. Furtado, E.M. A Onda Do Turismo Na Cidade Do Sol: A Reconfiguração Urbana de Natal. Available online: https://repositorio.ufrn.br/handle/123456789/13723 (accessed on 27 September 2023).
51. da Silva, F.R. Estudo Da Radiação Ultravioleta Na Cidade de Natal-RN. Ph.D. Thesis, Universidade Federal do Rio Grande do Norte, Natal, Brazil. Available online: https://oasisbr.ibict.br/vufind/Record/UFRN_54fe33d9c54657ddf7cceedfad43aa48 (accessed on 27 November 2023).
52. Instituto Nacional de Meteorologia (INMET). Normais Climatológicas Do Brasil 1961–1990. Available online: https://portal.inmet.gov.br/normais (accessed on 2 October 2023).
53. Neves, J.A. *Um Índice de Sustentabilidade Ao Fenômeno Da Seca Para O Semi-Árido Nordestino*; Repositorio UC: Santiago, Chile, 2010.
54. Bilbao, J.; Román, R.; Yousif, C.; Pérez-Burgos, A.; Mateos, D.; de Miguel, A. Global, Diffuse, Beam and Ultraviolet Solar Irradiance Recorded in Malta and Atmospheric Component Influences under Cloudless Skies. *Sol. Energy* **2015**, *121*, 131–138. [CrossRef]
55. Mckinlay, A.; DIffey, B. A Reference Action Spectrum for Ultraviolet Induced Erythema in Human Skin. Available online: https://hero.epa.gov/hero/index.cfm/reference/details/reference_id/57760 (accessed on 27 October 2023).
56. González-Rodríguez, L.; de Oliveira, A.P.; Rodríguez-López, L.; Rosas, J.; Contreras, D.; Baeza, A.C. A Study of UVER in Santiago, Chile Based on Long-Term in Situ Measurements (Five Years) and Empirical Modelling. *Energy* **2021**, *14*, 368. [CrossRef]
57. Davis Instruments. UV Sensor 6490 Vantage pro Espec Sheet. Available online: https://support.davisinstruments.com/article/qxi17f3woz-spec-sheet-solar-power-kit-heavy-duty-solar-power-kit-specifications-6612-6614 (accessed on 27 August 2023).
58. Levelt, P.F.; van den Oord, G.H.J.; Dobber, M.R.; Malkki, A.; Visser, H.; de Vries, J.; Stammes, P.; Lundell, J.O.V.; Saari, H. The Ozone Monitoring Instrument. *IEEE Trans. Geosci. Remote Sens.* **2006**, *44*, 1093–1101. [CrossRef]
59. Taipe, C.W.; Mendoza, E.G.; Flores, H.H. Validation of Ultraviolet Index Data from the Ozone Monitoring Instrument (OMI) Based on Measurements from Meteorological Stations in the City of Puno. *J. Phys. Conf. Ser.* **2021**, *1841*, 012005. [CrossRef]
60. Tanskanen, A.; Lindfors, A.; Määttä, A.; Krotkov, N.; Herman, J.; Kaurola, J.; Koskela, T.; Lakkala, K.; Fioletov, V.; Bernhard, G.; et al. Validation of Daily Erythemal Doses from Ozone Monitoring Instrument with Ground-Based UV Measurement Data. *J. Geophys. Res.* **2007**, *112*, 2. [CrossRef]
61. Jégou, F.; Godin-Beekmann, S.; Correa, M.P.; Brogniez, C.; Auriol, F.; Peuch, V.-H.; Haeffelin, M.; Pazmiño, A.; Saïag, P.; Goutail, F.; et al. Validity of Satellite Measurements Used for the Monitoring of UV Radiation Risk on Health. *Atmos. Chem. Phys.* **2011**, *11*, 13377–13394. [CrossRef]
62. Antón, M.; Cachorro, V.E.; Vilaplana, J.M.; Toledano, C.; Krotkov, N.A.; Arola, A.; Serrano, A.; de la Morena, B. Comparison of UV Irradiances from Aura/Ozone Monitoring Instrument (OMI) with Brewer Measurements at El Arenosillo (Spain)—Part 1: Analysis of Parameter Influence. *Atmos. Chem. Phys.* **2010**, *10*, 5979–5989. [CrossRef]
63. Kinne, S.; O'Donnel, D.; Stier, P.; Kloster, S.; Zhang, K.; Schmidt, H.; Rast, S.; Giorgetta, M.; Eck, T.F.; Stevens, B. MAC-V1: A New Global Aerosol Climatology for Climate Studies. *J. Adv. Model. Earth Syst.* **2013**, *5*, 704–740. [CrossRef]
64. Munro, R.; Lang, R.; Klaes, D.; Poli, G.; Retscher, C.; Lindstrot, R.; Huckle, R.; Lacan, A.; Grzegorski, M.; Holdak, A.; et al. The GOME-2 Instrument on the Metop Series of Satellites: Instrument Design, Calibration, and Level 1 Data Processing—An Overview. *Atmos. Meas. Tech.* **2016**, *9*, 1279–1301. [CrossRef]
65. Kujanpää, J.; Kalakoski, N. Operational Surface UV Radiation Product from GOME-2 and AVHRR/3 Data. *Atmos. Meas. Tech.* **2015**, *8*, 4399–4414. [CrossRef]
66. Liu, S.; Valks, P.; Beirle, S.; Loyola, D.G. Nitrogen Dioxide Decline and Rebound Observed by GOME-2 and TROPOMI during COVID-19 Pandemic. *Air Qual. Atmos. Health* **2021**, *14*, 1737–1755. [CrossRef]

67. Ialongo, I.; Arola, A.; Kujanpää, J.; Tamminen, J. Use of Satellite Erythemal UV Products in Analysing the Global UV Changes. *Atmos. Chem. Phys.* **2011**, *11*, 9649–9658. [CrossRef]
68. Chan, K.L.; Valks, P.; Heue, K.-P.; Lutz, R.; Hedelt, P.; Loyola, D.; Pinardi, G.; Van Roozendael, M.; Hendrick, F.; Wagner, T.; et al. Global Ozone Monitoring Experiment-2 (GOME-2) Daily and Monthly Level-3 Products of Atmospheric Trace Gas Columns. *Earth Syst. Sci. Data* **2023**, *15*, 1831–1870. [CrossRef]
69. Kalakoski, N. OMI UVB Level 2G HDF-EOS5 Format Specification Document. Available online: https://omi.fmi.fi/docs/OMUVB_L2_Format_Specification_Document_v2_6.pdf (accessed on 2 September 2023).
70. Sammes, P.; Noordhoek, R. OMI Algorithm Theoretical Basis Document Volume III. In *Clouds, Aerosols, and Surface UV Irradiance*; 2002. Available online: https://eospso.nasa.gov/sites/default/files/atbd/ATBD-OMI-03.pdf (accessed on 5 September 2023).
71. Força Aéra Brasileira (FAB). Como Decodificar O METAR E O SPECI?—Central de Ajuda DECEA. Available online: https://ajuda.decea.mil.br/base-de-conhecimento/como-decodificar-o-metar-e-o-speci/ (accessed on 27 October 2023).
72. Silva, A.A.; Souza-Echer, M.P. Ground-Based Observations of Clouds through Both an Automatic Imager and Human Observation. *Meteorol. Appl.* **2015**, *23*, 150–157. [CrossRef]
73. Reis, G.; Alves, S.; Bezerra, H.; Branches, R.; Silva, R.; Vaz Peres, L.; Pinheiro, D.K.; Lamy, K.; Benchérif, H.; Portafaix, T. Solar Ultraviolet Radiation Temporal Variability Analysis from 2-Year of Continuous Observation in an Amazonian City of Brazil. *Atmosphere* **2022**, *13*, 1054. [CrossRef]
74. de Paula, M.; Godin-Beekmann, S.; Haeffelin, M.; Brogniez, C.; Verschaeve, F.; Saiag, P.; Pazmino, A.; Mahé, E. Comparison between UV Index Measurements Performed by Research-Grade and Consumer-Products Instruments. *Photochem. Photobiol. Sci.* **2010**, *9*, 459–463. [CrossRef]
75. Glen, S. Correlation Coefficient: Simple Definition, Formula, Easy Calculation Steps. Available online: https://www.statisticshowto.com/probability-and-statistics/correlation-coefficient-formula (accessed on 25 August 2023).
76. Akoglu, H. User's Guide to Correlation Coefficients. *Turk. J. Emerg. Med.* **2018**, *18*, 91–93. [CrossRef] [PubMed]
77. Chicco, D.; Warrens, M.J.; Jurman, G. The Coefficient of Determination R-Squared Is More Informative than SMAPE, MAE, MAPE, MSE and RMSE in Regression Analysis Evaluation. *PeerJ Comput. Sci.* **2021**, *7*, e623. [CrossRef] [PubMed]
78. Barbieri, F.; Rajakaruna, S.; Ghosh, A. Very Short-Term Photovoltaic Power Forecasting with Cloud Modeling: A Review. *Renew. Sustain. Energy Rev.* **2017**, *75*, 242–263. [CrossRef]
79. Sathishkumar, V.E.; Ramu, A.G.; Cho, J. Machine Learning Algorithms to Predict the Catalytic Reduction Performance of Eco-Toxic Nitrophenols and Azo Dyes Contaminants (Invited Article). *Alex. Eng. J.* **2023**, *72*, 673–693. [CrossRef]
80. Lillo-Bravo, I.; Vera-Medina, J.; Fernández-Peruchena, C.M.; Pérez-Aparicio, E.; López-Álvarez, J.A.; Delgado-Sanchez, J.M. Random Forest Model to Predict Solar Water Heating System Performance. *Renew. Energy* **2023**, *216*, 119086. [CrossRef]
81. Coariti, J.R. Características Da Radiação Ultravioleta Solar E Seus Efeitos Na Saúde Humana Nas Cidades de La Paz–Bolívia E Natal–Brasil. Ph.D. Thesis, Universidade Federal do Rio Grande do Norte, Natal, Brazil, 2017.
82. Lamy, K.; Portafaix, T.; Brogniez, C.; Lakkala, K.; Pitkänen, M.R.A.; Arola, A.; Forestier, J.-B.; Amélie, V.; Abdoulwahab Toihir, M.; Rakotoniaina, S. UV-Indien Network: Ground-Based Measurements Dedicated to the Monitoring of UV Radiation over the Western Indian Ocean. *Earth Syst. Sci. Data* **2021**, *13*, 4275–4301. [CrossRef]
83. Alvares, C.A.; Stape, J.L.; Sentelhas, P.C.; de Moraes Gonçalves, J.L.; Sparovek, G. Köppen's Climate Classification Map for Brazil. *Meteorol. Z.* **2013**, *22*, 711–728. [CrossRef]
84. Cede, A.; Blumthaler, M.; Luccini, E.; Piacentini, R.D.; Nuñez, L. Effects of Clouds on Erythemal and Total Irradiance as Derived from Data of the Argentine Network. *Geophys. Res. Lett.* **2002**, *29*, 76-1–76-4. [CrossRef]
85. de Oliveira, P.T.; Silva CM, S.E.; Lima, K.C. Linear Trend of Occurrence and Intensity of Heavy Rainfall Events on Northeast Brazil. *Atmos. Sci. Lett.* **2013**, *15*, 172–177. [CrossRef]
86. EPA (Unites States Environmental Protection Agency). UV Index Scale. Available online: https://19january2017snapshot.epa.gov/sunsafety/uv-index-scale-1_.html (accessed on 23 August 2023).
87. Mohamed, M.S.; Abdel, M.; El-Metwally, M.; El-Nobi, E.F. Validation of UV-Index Retrieved from Three Satellites against Ground-Based Measurements at Different Climates in Egypt. *Egypt. J. Remote Sens. Space Sci.* **2023**, *26*, 361–367. [CrossRef]
88. Pitkänen MR, A.; Arola, A.; Lakkala, K.; Koskela, T.; Lindfors, A.V. Comparing OMI UV Index to Ground-Based Measurements at Two Finnish Sites with Focus on Cloud-Free and Overcast Conditions. *Egypt. J. Remote Sens. Space Sci.* **2015**, *8*, 487–516. [CrossRef]
89. Bernhard, G.; Arola, A.; Dahlback, A.; Fioletov, V.; Heikkilä, A.; Johnsen, B.; Koskela, T.; Lakkala, K.; Svendby, T.M.; Tamminen, J. Comparison of OMI UV Observations with Ground-Based Measurements at High Northern Latitudes. *BIBSYS Brage* **2015**, *15*, 7391–7412. [CrossRef]